

## <sup>1</sup>H NMR Study of mono- and di-cyanide ligated Hemin Complexes as Models of Hemoproteins

Kang-Bong Lee<sup>1</sup>, Nam Jun Kim\*, Jeehye Kweon, Jae-Seong Rhee, Young-Sang Choi\*

Advanced Analysis Center, Korea Institute of Science and Technology, P. O. Box 131, Cheongryang, Seoul 130-650

\*Department of Chemistry, Korea University, 1, 5<sup>st</sup>, Anam-Dong, Sungbuk-Ku, Seoul 136-701

(Received Oct. 4, 1994)

### Heme 단백질의 Model로서의 Hemin 착물에 관한 <sup>1</sup>H NMR 연구

이강봉<sup>1</sup> · 김남준\* · 권지혜 · 이재성 · 최영상\*

한국과학기술연구원 특성분석센터

\*고려대학교 화학과

(1994. 10. 4. 접수)

**Abstract :** <sup>1</sup>H NMR spectra for monocyanide ligated ferriprotoporphyrin(hemin) complex and dicyanide coordinated hemin complex in dimethylsulfoxide(DMSO-d<sub>6</sub>) solution have been recorded and analyzed. NMR spectra of hemin-cyanide complexation in DMSO-d<sub>6</sub> exhibit that the cyanide ligation to hemin is temperature-dependent. Thermodynamic parameters for the monocyanide ligated hemin to dicyanide ligated hemin are consistent with endothermic process with  $\Delta H^\circ = 736.6 \text{ cal/mol}$  and  $\Delta S^\circ = 16.4 \text{ eu}$ . Detailed analysis of the anomalous deviation from Curie behavior for CN/DMSO coordinated hemin complex demonstrates the presence of a high spin character, and this weaker axial field relative to the purely low-spin dicyanide hemin complex is supposed to attribute to instantaneously ruptured iron-DMSO bond. This complex may serve as a useful model to characterize electronic/molecular structure of hemoproteins, which one of axial ligands is weak.

**요약 :** DMSO(dimethylsulfoxide-d<sub>6</sub>) 용액 속에 존재하는 CN/CN 리간드의 hemin 착물과 CN/DMSO의 hemin 착물이 <sup>1</sup>H NMR로 기록되어지고 분석되어졌다. Hemin으로의 CN 착물화 과정은 온도에 따라 변화함을 NMR 스펙트럼이 보여 주며, 한 개의 CN 리간드에서 두 개의 CN 리간드착물로 바뀌는 과정의 열역학함수는  $\Delta H^\circ = 736.6 \text{ cal/mol}$  및  $\Delta S^\circ = 16.4 \text{ eu}$ 인 흡열과정을 나타낸다. CN/DMSO의 hemin 착물은 Curie behavior로부터의 벗어남은 high-spin 성격의 존재를 나타내고, 이는 Fe-DMSO 결합이 순간적으로 깨짐을 의미하며, 이러한 CN/DMSO hemin 착물이 한 개의 axial ligand가 약한 heme 단백질의 전자 및 분자구조의 model complex로 작용할 수 있음을 보여 준다.

**Key words :** <sup>1</sup>H NMR, Hemin complex

#### Introduction

NMR spectra of paramagnetic transition-metal

complexes yield valuable information on magnetic and electronic properties of the metal center, as well as on the nature and extent of metal-ligand co-

valency.<sup>1,2</sup> The iron complexes of the cyclic tetrapyrroles, the porphyrins are a particularly important group of complexes. All of the commonly accessible oxidation/spin states are paramagnetic, and the detailed patterns of the hyperfine shifts for the tetrapyrrole have been shown to be essentially diagnostic for a given oxidation/spin/ligation state of the iron.<sup>3-5</sup> The close parallel between hyperfine shift patterns of iron tetrapyrrole complexes and the intact hemoproteins with the same chromophore has made the simple complexes ideal models for elucidating protein-based spectral perturbations in the latter systems. Moreover, the asymmetric functionalization of the tetrapyrrole periphery leads to redistribution of the delocalized spin density that provide us with one of most sensitive methods for mapping ligand molecular orbitals.<sup>7-9</sup> The characterization of the in-plane asymmetry in paramagnetic heme complexes using NMR involves a detailed analysis of the origin of the isotropic shifts in terms of possible magnetic anisotropy and transferred unpaired spin density. The isotropic shift for a nucleus in a complex or protein is given by

$$(\Delta H/H)_{\text{iso}} = (\Delta H/H)_{\text{con}} + (\Delta H/H)_{\text{dip}} \quad (1)$$

where the contact shift is

$$(\Delta H/H)_{\text{con}} = -Ag\beta S(S+1)/(\gamma k\pi)3kT \quad (2)$$

and the dipolar shift is represented by

$$(\Delta H/H)_{\text{dip}} = 1/3N\{[\chi_z - 1/2(\chi_x + \chi_y)](3\cos^2\theta - 1)/r^3 + 3/2(\chi_x - \chi_y)\sin^2\theta\cos^2\Omega\} \quad (3)$$

where  $A$  is the Fermi contact coupling,  $\chi_x$ ,  $\chi_y$ ,  $\chi_z$  are the principal components of the susceptibility tensor,  $\theta$  is the angle between the metal-nucleus vector and the  $z$  axis,  $r$  is the length of this vector, and the  $\Omega$  is the angle between the projection of  $r$  on the  $xy$  plane and the  $x$  axis.

In-plane asymmetry can arise from either differences in  $A$  (transferred spin to individual pyrroles) or rhombic magnetic anisotropy (i. e., the

second term in eq. 3). Since low-spin ferric systems are known to be magnetically anisotropic, both cases must be considered.

The most serious barrier to the full utilization of the NMR spectral information in paramagnetic model complexes is the unambiguous assignment of the resonances, since the hyperfine shifts invalidate the functional group/shift correlation of diamagnetic systems and generally paramagnetic relaxation obscures multiplet structure. The assignment strategies have relied on  $^1\text{H}$ - $^1\text{H}$  COSY which detect the characteristic spin (scalar) connectivity of peripheral substituents of tetrapyrrole complexes.<sup>10</sup>

Heme model complex and ferric hemoproteins in a given spin ground state invariably exhibit Curie-like behavior for the majority of hyperfine-shifted resonances, and strong and systematic deviations from Curie behavior are generally taken as direct evidence for a spin equilibrium.<sup>11</sup>

Thus, the electronic structure for the mono- and di-cyanide hemins, temperature-dependent behavior for the NMR signals of mono- and di-cyanide hemins and the thermodynamic parameters for the equilibrium of cyanide ligand binding to the iron of heme as models of hemoproteins will be documented in this report.

## Experimental Section

**Sample preparation :** Protoporphyrin IX iron(III) was used as purchased from Sigma without further purification. The low spin bis-cyano and mono-cyano complexes were prepared by dissolving the appropriate porphyrin iron chloride with 1:1.5 potassium cyanide in  $(\text{C}^2\text{H}_5)_2\text{SO}$  in the 5mm NMR tube. Sample concentration was about 10mM.

**NMR spectroscopy :**  $^1\text{H}$  NMR spectra were collected on Bruker AM-200 spectrometers operating in quadrature mode at 200-MHz. All 1D spectra were collected by using a standard one-pulse experiment, with a presaturation pulse when necessary to suppress the solvent signal, and with 5T<sub>1</sub>.

interpulse delay. Typical spectra resulted from collecting ~256 on 16384 data points over 7000Hz bandwidth at a repetition rate of  $0.4 \text{ sec}^{-1}$ . To improve signal to noise ratio, the free induction decays were apodized, which introduced 2 Hz line broadening. Chemical shifts for all spectra are referenced to the residual solvent line. NMR spectra were recorded in  $10^\circ\text{C} (\pm 0.1^\circ\text{C})$  intervals over the temperature range  $24 \sim 55^\circ\text{C} (\pm 0.1^\circ\text{C})$ . Nonselective  $T_{1s}$  were obtained from the initial slope of the semilogarithmic plots of the intensity data from an inversion-recovery experiment using a composite  $180^\circ$  pulse: for incompletely resolved lines,  $T_{1s}$  were calculated from the delay time which produced a null,  $\tau_{\text{null}}$ , by the relation  $T_1 = \tau_{\text{null}} / \ln 2$ . For 2D spectra, an n-type magnitude COSY, M-COSY, sequence was used, with a presaturation pulse during the relaxation delay to suppress the solvent resonance when necessary. The  $90^\circ$  pulse for  $^1\text{H}$  was  $7 \sim 8 \mu\text{s}$ . 2D  $^1\text{H}$ - $^1\text{H}$  COSY spectrum was collected with 1024 points in  $t_2$  over the minimum bandwidth necessary to include all peaks with expected spin connectivities and centered about the solvent resonance when possible. The number of  $t_2$  data points were chosen with the consideration of needing at least  $2T_2$  ms for acquisition time length, where  $T_2$  is the longest  $T_2$  value for the complex as estimated from the linewidth for all peaks in the 1D reference spectrum. Resulting acquisition time for 2D spectrum shown was 10.2 ms. The repetition rate of the pulse sequences utilized was  $0.65 \text{ s}^{-1}$  following the guideline of  $1.5T_1$ . Accordingly, pulse delays selected was 1.5 sec. 2D experiment includes 4 dummy scans prior collection of each block.  $256t_1$  blocks were collected with 128 scans per block.

## Results and Discussion

**Equilibrium in heme-cyanide system :** Fig. 1 shows the proton NMR spectra for the diverse ligand states of hemin at various potassium cyanide concentrations. In the absence of cyanide (Fig 1A),

only the high spin hemin which has DMSO as its fifth and sixth ligands exists in the solution. The signals of high spin hemin complex exhibit a large paramagnetic shift to low field at  $50 \sim 70$  ppm (shown in inset of Fig. 1A). Upon addition of cyanide to the solution, the intensity of these resonances from high spin hemin decrease and finally disappear with the concomitant appearance of a new group of resonance peaks at  $7 \sim 18$  ppm. These new peaks which come from monocyanoide hemin reach maximum intensity at a cyanide-hemin ratio of about 1 : 1 and then decrease thereafter, finally disappearing at about a 3 : 1 ratio, which gives only low spin dicyanide complex as shown in a series of spectra of Fig. 1. The paramagnetic shifts of methyls in monocyanoide hemin complex (mixed ligand complexes) is smaller than those of dicyanide hemin complex and peaks in the former case are shifted upfield relative to those of later case. This could either indicate a larger magnetic anisotropy (larger positive dipolar shifts) or smaller contact contributions to the isotropic shifts of monocyanoide hemin complex. It should also be pointed out a fact that the exchange rate of the mixed-ligand complexes is slow on the NMR time scale. This has been demonstrated clearly in an earlier investigation of the  $\text{CN}^-$  equilibria of monodicyanidehemin complex.<sup>12</sup>

**Mono- and di-cyanide hemin complexes :** Fig. 2 illustrates the 200-MHz  $^1\text{H}$  NMR spectrum for the mixed ligand state hemins, dicyanidehemin-monocyanoidehemin ratio of about 1 : 1. This state is reached when hemin-cyanide ratio is about 1 : 1.5. The resonances from dicyanidehemin and monocyanoidehemin are labeled as capital letters and lower case letters, respectively. As shown previously, the chemical shifts of the signals from the dicyanidehemin complex in  $\text{DMSO-d}_6$  solvent are very much the same to those of dicyanoheemin complex in  $\text{CD}_3\text{OD}$  solvent. Although one of the ligand binding site is ligated by a weak ligand, DMSO in the case of monocyanoheemin, the chemical shift dis-

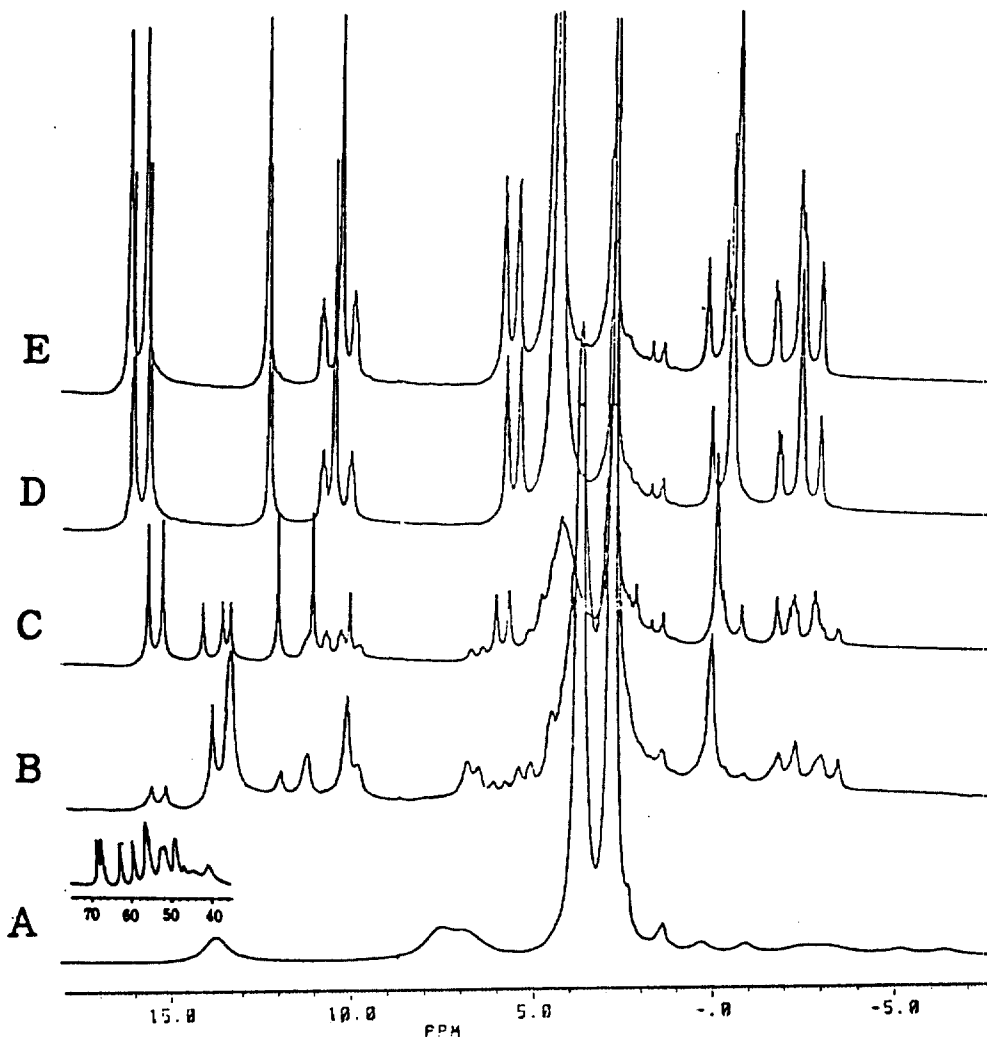


Fig. 1. 200 MHz  $^1\text{H}$  NMR spectra of 10 mM ferriprotoporphyrin(hemin) in  $\text{DMSO-d}_6$  solution at various potassium cyanide concentrations. The potassium cyanide concentrations are (A) 0.0 mM. The low field region of high spin hemin complex is given in the inset. (B)  $\sim 10$  mM (C)  $\sim 20$  mM (D)  $\sim 30$  mM (E)  $\sim 40$  mM

persion is very similar to that of dicyanohemin complex. The complete 200MHz M-COSY map recorded at ambient temperature and illustrated in Fig. 3. All expected cross peaks are observed between hyperfine-shifted scalar coupling protons, which are geminal and vicinal protons in heme vinyl and propionate groups (The structure and the labeling system of the heme are given in the inset of Fig. 3).

Cross peaks 1 and 2 indicates the scalar

interactions in  $2V_\alpha/2V_{\beta_c}$ (m, 1) and  $2V_\alpha/2V_{\beta_t}$ (m, 2) in monocyanoheemin complex, respectively. Continuing clockwise, we obtain  $2V_\alpha/2V_{\beta_t}$ (d, 3),  $4V_\alpha/4V_{\beta_t}$ (d, 4),  $4V_\alpha/4V_{\beta_t}$ (m, 5),  $4V_\alpha/4V_{\beta_c}$ (m, 6),  $4V_\alpha/4V_{\beta_t}$ (d, 7),  $2V_\alpha/2V_{\beta_c}$ (d, 8). m and d in parenthesis denote monocyanoheemin and dicyanoheemin complexes, respectively and numbers in parenthesis indicates the numbering from 2-D map of Fig. 3. In order to differentiate the signals between monocyanoheemin and dicyanoheemin complexes,

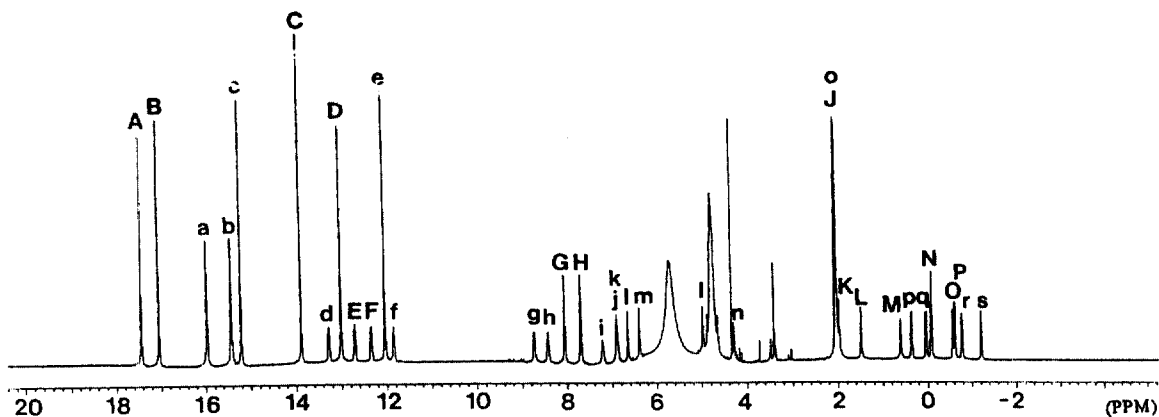


Fig. 2. Optimally resolved 200-MHz  $^1\text{H}$  NMR trace for the 10 mM monocyanide and dicyanide hemin complex in  $\text{DMSO-d}_6$  at  $25^\circ\text{C}$ . The signals from dicyanidehemin and monocyanidehemin are labeled as capital letters and lower case letters, respectively.

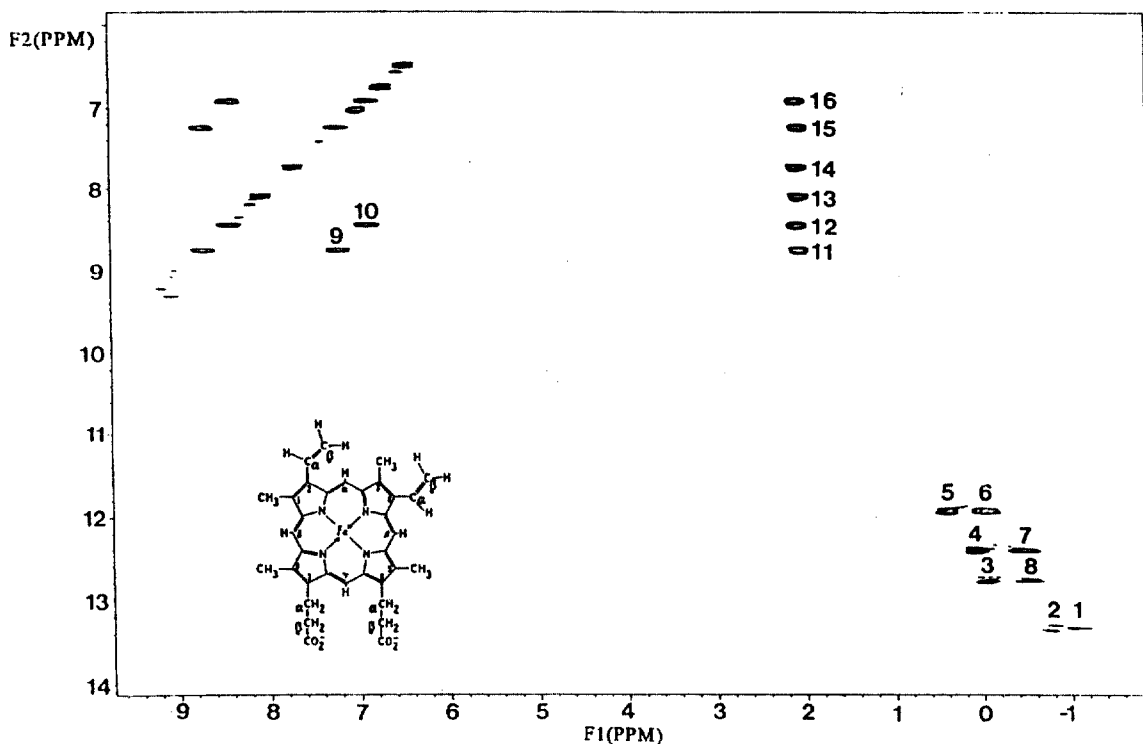


Fig. 3. 200-MHz M-COSY map of mono- and di-cyanide hemin complexes in  $\text{DMSO-d}_6$  at  $25^\circ\text{C}$ . Cross peaks connecting propionate and vinyl groups are illustrated. The collected data consist of 128  $t_1$  blocks of 2048 scans each with 1024  $t_2$  points over a 6000 Hz bandwidth for acquisition times in  $t_1$  and  $t_2$  of 10 ms and 20 ms, respectively. The optimal map resulted from apodizing over  $1024 \times 1024$  points prior to zero-filling in  $t_1$  for a final digitization of 49 Hz/points.

cyanide titration method was utilized as shown in Fig. 1. and the assignment strategy for dicyanide-hemin complex was based on the chemical shift pattern of the equivalent complex in CD<sub>3</sub>OD solvent as published earlier.<sup>3</sup> Cross peaks 9 and 10 are due to the scalar interactions of  $7P_x/7P_x^1$ (m, 9) and  $6P_x/6P_x^1$ (m, 10), respectively. The absence of strong cross peaks for  $6P_x/6P_x^1$ (d) and  $7P_x/7P_x^1$ (d) suggests that two peaks must be essentially degenerate between two geminal partner protons. Cross peaks 11~16 are from scalar couplings of  $6P_x/6P_\beta$ (m, 11),  $7P_x/7P_\beta$ (m, 12),  $6P_x/6P_\beta$ (d, 13),  $7P_x/6P_\beta$ (d, 14),  $6P_x^1/6P_\beta^1$ (m, 15), and  $7P_x^1/7P_\beta^1$ (d, 16), respectively. The M-COSY map data in Fig. 3

clearly show that coherence is detectable in paramagnetic iron complex, essentially all spin connectivities were detected that could be expected for an analogous diamagnetic system. The chemical shifts for monocyano-hemin and dicyano-hemin complexes are listed in Table I and Table II, respectively. Direct determination of nonselective T<sub>1</sub> values for resolved resonances by the inversion-recovery technique yielded the values in Table I and Table II.

The chemical shifts of mean meso protons at 25°C for the dicyano-hemin complex and monocyano-hemin complex are 2.25 ppm and 6.05 ppm, respectively and this ~4 ppm chemical shift difference is con-

Table I. <sup>1</sup>H NMR peak assignment and T<sub>1</sub> relaxation time of dicyanide ligated hemin in DMSO solution at 25°C.

Labels	Chemical Shift(ppm)	Peak Assignment	T1 relaxation time(ms)
A	17.43	8-CH <sub>3</sub>	172.1
B	17.04	5-CH <sub>3</sub>	178.7
C	13.88	3-CH <sub>3</sub>	218.2
D	13.00	1-CH <sub>3</sub>	214.2
E	12.70	2-V <sub>α</sub>	228.5
F	12.34	4-V <sub>α</sub>	228.5
G	8.05	6-P <sub>α</sub> 6-P <sub>α</sub> <sup>1</sup>	140.5
H	7.69	7-P <sub>α</sub> 7-P <sub>α</sub> <sup>1</sup>	142.4
I	4.97	γ-meso	56.6
J	2.03	6-P <sub>β</sub> 6-P <sub>β</sub> <sup>1</sup> 7-P <sub>β</sub> 7-P <sub>β</sub> <sup>1</sup>	126.1
K	1.97	β-meso	61.5
L	1.47	δ-meso	53.5
M	0.60	α-meso	49.0
N	-0.09	4-V <sub>βt</sub> 2-V <sub>βt</sub>	215.7
O	-0.58	4-V <sub>βc</sub>	245.3
P	-0.63	2-V <sub>βc</sub>	242.6

Table II.  $^1\text{H}$  NMR peak assignment and  $T_1$  relaxation time of monocyanoide ligated hemin in DMSO solution at  $25^\circ\text{C}$ .

Labels	Chemical shift(ppm)	Peak Assignment	$T_1$ relaxation time(ms)
a	15.96	8- $\text{CH}_3$	136.2
b	15.42	5- $\text{CH}_3$	140.9
c	15.20	3- $\text{CH}_3$	167.9
d	13.28	2- $\text{V}_x$	176.1
e	12.04	1- $\text{CH}_3$	171.1
f	11.85	4- $\text{V}_x$	165.5
g	8.73	6- $\text{P}_x$	96.8
h	8.42	7- $\text{P}_x$	97.2
i	7.21	6- $\text{P}_\alpha^1$	93.0
j/k	6.89	7- $\text{P}_x^1$ $\gamma$ -meso	60.6
l	6.64	$\beta$ -meso	47.1
m	6.38	$\delta$ -meso	47.3
n	4.29	$\alpha$ -meso	63.6
o	2.03	6- $\text{P}_\beta$ 6- $\text{P}_\beta^1$ 7- $\text{P}_\beta$ 7- $\text{P}_\beta^1$	126.1
p	0.36	4- $\text{V}_{\beta t}$	185.8
q	0.03	4- $\text{V}_{\beta c}$	201.1
r	-0.79	2- $\text{V}_{\beta t}$	183.2
s	-1.23	2- $\text{V}_{\beta c}$	216.0

sidered to be due to the minor portion of high spin character in monocyanoheemin complex.

**Temperature dependence :** The hyperfine shifts of dicyanoheemin complex in  $\text{DMSO-d}_6$  solvent displayed very similar behavior when compared to the same complex in methanol solvent as shown in the Curie plot Fig. 4. As expected by the Curie law, the heme methyl signals in dicyanoheemin complex displayed decreased shift at higher temperatures, which means that the electronic property of iron in dicyanoheemin complex in  $\text{DMSO-d}_6$  is the same

with that of equivalent complex in  $\text{CD}_3\text{OD}$  solvent. The temperature dependence of the vinyl protons shows anti-Curie behavior, probably because there is a change in the average out-of-plane twisting of the vinyl group with temperature. Thus, low-spin myoglobin and cytochrome  $b_5$  locked sterically with the adjacent  $\text{CH}_3$  groups and protein matrix may cause the vinyls to be more perpendicular to the plane of the porphyrin ring, thus allowing them less spin delocalization in the low-spin heme protein which leads to Curie behavior. However, the

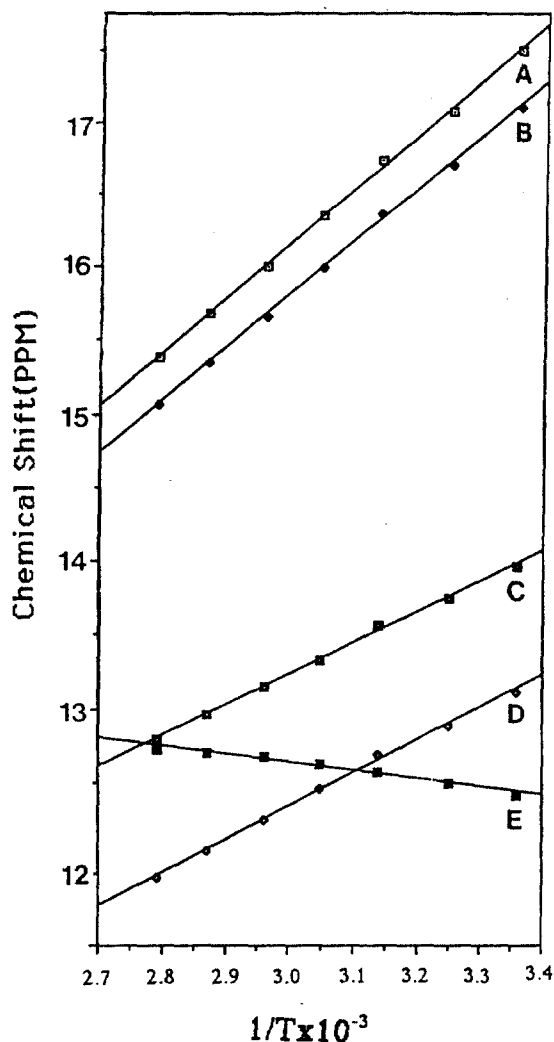


Fig. 4. Plot of observed chemical shifts versus reciprocal absolute temperature (Curie plot) of 10 mM dicyanidehemin complex in DMSO- $d_6$  at 25°C for the selected signals (A, 8-CH<sub>3</sub>; B, 5-CH<sub>3</sub>; C, 3-CH<sub>3</sub>; D, 1-CH<sub>3</sub>; E, 2-V<sub>α</sub>).

hyperfine shifts of monocyanoheemin complex in DMSO- $d_6$  illustrated rather remarkably anomalous behavior when compared to the well-characterized dicyanoheemin complex as shown in Fig. 4. Although the hyperfine shifts of 8-CH<sub>3</sub>, 5-CH<sub>3</sub> and 3-CH<sub>3</sub> decrease at elevated temperatures as expected by the Curie law, the temperature profiles of the various resonances in Fig. 5

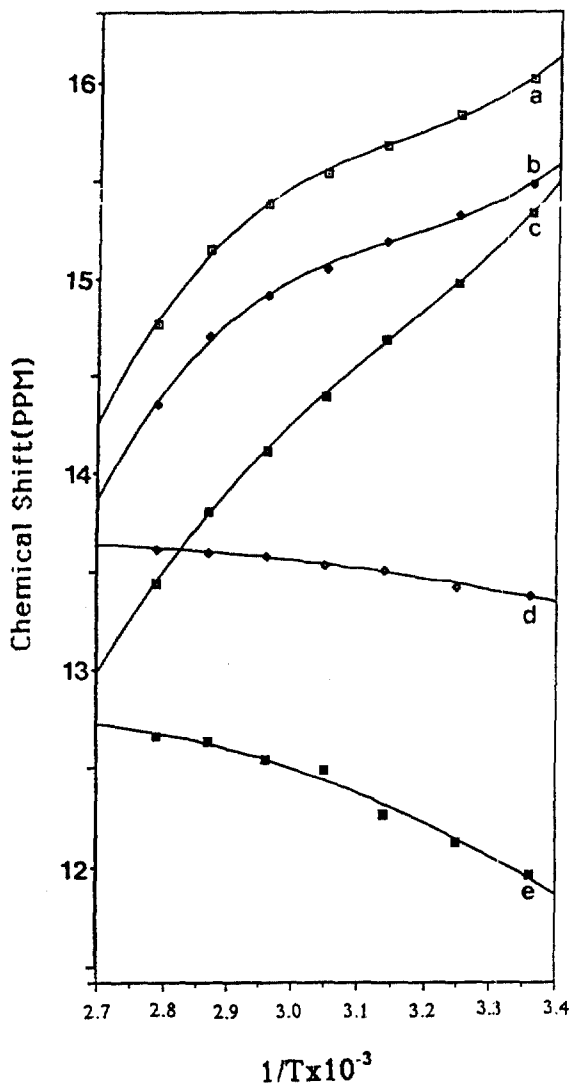


Fig. 5. Plot of observed chemical shifts versus reciprocal absolute temperature (Curie plot) of 10 mM monocyanoheemin complex in DMSO- $d_6$  at 25°C for the selected signals (a, 8-CH<sub>3</sub>; b, 5-CH<sub>3</sub>; c, 3-CH<sub>3</sub>; d, 1-CH<sub>3</sub>; e, 2-V<sub>α</sub>).

illustrates the curvature as shown in structurally less characterized, spin-equilibrated cytochromes. The hyperfine shifts of 2V<sub>α</sub> and 1-CH<sub>3</sub> increase as temperature is raised, which leads to anti-Curie behavior in conjunction with the curvature. The unusual temperature dependence can be explained by the severe contribution from dipolar interaction between unpaired electron of iron and protons.



The detailed theory indicates that dipolar shifts arising from the zero-field splitting (ZFS) have a characteristic  $T^2$  dependence for high spin  $d^5$  ions, in contrast to the  $T^{-1}$  dependence of the contact contribution to the shift. Thus, the shift for high-spin (III) can be written in the form

$$(\Delta H/H)^{\text{iso}} = \alpha/T + \varepsilon/T^2$$

where  $\alpha = 35g\beta A/12k\gamma_H$ ,  $\varepsilon = (28g^2\beta^2 D/9k^2)(3\cos^2\theta - 1)/r^3$  and  $D$  is the ZFS parameter. The  $T^{-2}$  term represents the dipolar contribution. From relative geometric factors, the dipolar contribution at any other position in the complex can be determined.<sup>1</sup>

Ferric hemoprotein in a given ground state invariably exhibit Curie-like behavior for the majority of hyperfine-shifted resonances, and strong and systematic deviations from Curie behavior are generally taken as direct evidence for a spin-state equilibrium. The present observation of anti-Curie behavior for the heme methyls, together with their low temperature shifts, clearly dictates the presence of a low-spin ( $S=1/2$ ) ground state in rapid equilibrium with a thermally accessible high-spin ( $S=5/2$ ) state. The nature of the deviations from Curie behavior for different resonances in such an equilibrium depends on their relative shift differences in the low-spin,  $S=1/2$ , and high-spin,  $S=5/2$ , states. Protons with larger shifts of the same direction in high-spin than in low-spin form would exhibit anti-Curie behavior because of the larger effect of populating the high-spin state than the  $T^{-1}$  change of the low-spin state.

Two possibilities for the high-spin state must be considered, a six-coordinate state where the spin equilibrium is within an invariant ligation state [such as for an intermediate ligand field observed for methoxy-metazidomyoglobin] or a five-coordinate state where one ligand, DMSO-iron bond ruptured. The largely contact shift patterns for heme is highly characteristic of the ligation state,

differing primarily in the meso-H shift direction.

#### Monocyanidehemin-dicyanide hemins equilibrium

The observation of transition from monocyanidehemin to dicyanidehemin as a function of cyanide concentration was shown above. Likewise, observation of temperature-dependent monocyanide-dicyanidehemin complex equilibrium will yield data which can be used to determine the thermodynamic parameters of two entities in equilibrium. The rate of exchange among the two hemin species is slow on the NMR time scale



$$K = [\text{Hemin}(\text{CN})_2^-] / [\text{Hemin}(\text{CN})][\text{CN}^-]$$

The observation of transition from monocyanidehemin to dicyanidehemin in  $\text{DMSO-d}_6$  is

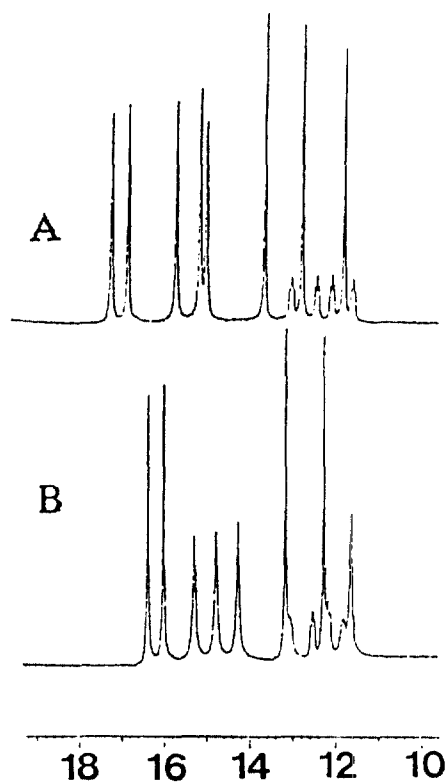


Fig. 6. 200 MHz  $^1\text{H}$  NMR spectra of 10mM ferriprotoporphyrin(hemin) in  $\text{DMSO-d}_6$  solution at (A) 25°C and (B) 45°C.

illustrated in Fig. 6. Fig. 6 shows that the signal intensity for dicyanide hemin complex increase dramatically in compensation for decrease of the signal intensity of monocyano-hemim complex at elevated temperature. A plot of  $\ln K$ . vs.  $T^{-1}$  yields the expected straight line, shown in Fig. 7. The ratio of  $[\text{Hemin}(\text{CN})_2]/[\text{Hemin}(\text{CN})][\text{CN}^-]$  is calculated from the NMR signal intensity ratio of two different complexes and the concentration of free  $\text{CN}^-$  was taken from the reference at 25°C. The plot yields the thermodynamic parameters  $\Delta H^\circ = 736.6 \text{ cal/mol}$ ,  $\Delta S^\circ = 16.4 \text{ eu}$ . The positive  $\Delta H^\circ$

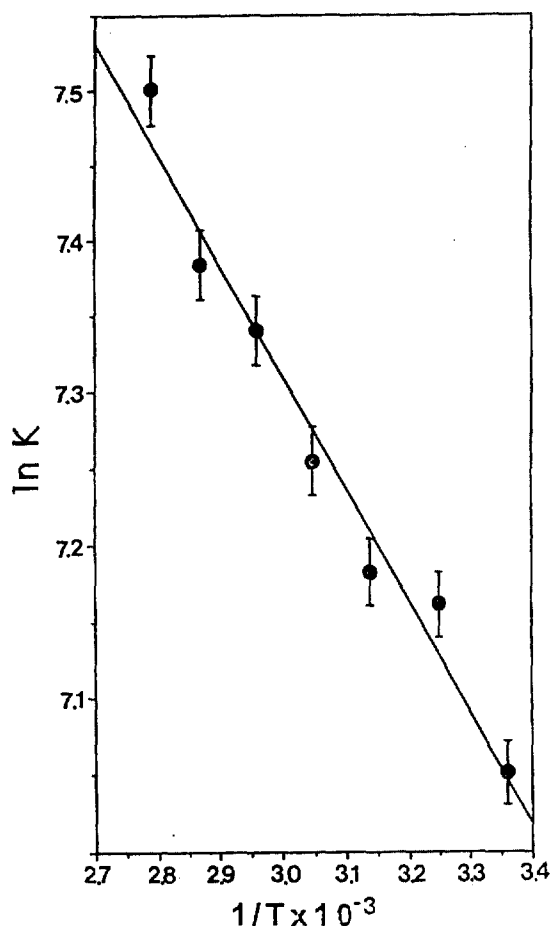


Fig. 7. Van't Hoff plot for the monocyano-hemim complex to dicyano-hemim complex equilibrium in DMSO- $d_6$ .  $\Delta H^\circ = 736.6 \text{ cal/mol}$ ,  $\Delta S^\circ = -4150.6 \text{ cal/mol}$ ,  $\Delta G^\circ = -4150.6 \text{ cal/mol}$ .

shows that the monocyano-hemim complex goes to the dicyano-hemim complex as temperature is raised, which is endothermic reaction and the positive  $\Delta H^\circ$  is consistent with the fact that the reaction above is a natural process.

**Biological implications :** The thermally accessible six-coordinate spin equilibrium in monocyano-hemim complex is in contrast to the behavior observed for the dicyano-hemim complex, this low spin  $\rightleftharpoons$  high spin equilibria for ferric hemoproteins are not uncommon, although only infrequently observed among other cytochromes with axial His/Met ligation and demands that the effective axial field (i. e. Fe-DMSO bond) is weakened in the present monocyano-hemim complex. Previously reported NMR spectra of structurally characterized ferricytochromes with His/Met ligation exhibit anti-Curie behavior indicative of a low-spin ferric state.<sup>13</sup> Therefore, the elucidation for the electronic/molecular structure and ligation state of monocyano-hemim complex will shed light on the characterization of those of hemoproteins, which one of axial ligands is weak. The next step will be to implement  $^{13}\text{C}$  NMR studies to establish the relationship of the  $^{13}\text{C}$  NMR parameters and spin equilibrated paramagnetism. These studies are in progress.

**Acknowledgment :** This work was supported by grants from the Ministry of Science and Technology.

#### References

1. La Mar, G. N., Horrocks, Jr., W. D., Holm, R. H., Eds., "NMR of Paramagnetic Molecules": New York, 1973.
2. Bertini, I. Luchinat, C. "NMR of Paramagnetic Molecules in Biological Systems": Benjamin/Cummings: Menlo Park, CA, 1986.
3. La Mar, G. N., Walker, F. A. "The Porphyrins: Academic press": New York, Vol. 4, p. 61.
4. La Mar, G. N. In "Biological Applications of

- Magnetic Resonance": Shulman, R. G., Ed.: Academic Press: New York, 1979: p. 305.
5. Latos-Grazynski, L., Balch, A. L., La Mar, G. N. *Adv. Chem. Ser.*, **201**, 661(1982).
  6. Satterlee, J. D. *Annu. Rep. NMR Spectrosc.* **17**, 79(1986).
  7. La Mar, G. N., Viscio, D. B., Smith, K. M., Caughey, W. S., Smith, M. L. *J. Am. Chem. Soc.*, **100**, 8085(1978).
  8. Latos-Grazynski, L., Cheng, R. -J., La Mar, G. N., Balch, A. L. *J. Am. Chem. Soc.*, **103**, 4270 (1981).
  9. Balch, A. L., Chan, Y. W., La Mar, G. N., Latos-Grazynski, L., Renner, M. W. *Inorg. Chem.*, **24**, 1437(1985).
  10. Keating, K. A., de Ropp, J. A., La Mar, G. N., Balch, A. L., Shiau, F. Y., Smith, K. M. *Inorg. Chem.*, **30**, 3258(1991).
  11. Iizuka, T., Morishima, I. *Biochim. Biophys. Acta.*, **371**, 1(1974).
  12. Wang, J. T., Yeh, H. J. C. Johnson, D. F. *J. Am. Chem. Soc.*, **97**, 1968(1975).
  13. Wu, J. -Z., La Mar, G. N., Yu, L., Lee, K. -B., Walker, F. A., Chiu, M. L., Sligar, S. G. *Biochemistry*, **30**, 2156(1991).